Available online at www.sciencedirect.com
ScienceDirect
Journal of the European Ceramic Society 29 (2009) 2559–2565
www.elsevier.com/locate/jeurceramsoc

Synthesis, sintering and electrical properties of yttria–calcia-doped ceria

A. Moure, J. Tartaj, C. Moure *

Instituto de Cerámica y Vidrio, CSIC, Electroceramics Department, c/Kelsen No. 5, Cantoblanco, 28049 Madrid, Spain

Received 21 January 2009; accepted 20 February 2009
Available online 25 March 2009

Abstract

Crystalline yttria and calcia doped ceria powder, with a composition of $Ce_{0.8}Y_{0.18}Ca_{0.02}O_{2-\delta}$ has been prepared by a coprecipitation procedure from the corresponding nitrates of component cations. Nanopowder was obtained after thermal treatment at 700 °C 2 h of the coprecipitated mixtures. Specific surface area was 45 m^2/g. Isostatically and uniaxially pressed pellets were prepared from the powder. Sintering behaviour was followed by CHR dilatometer. Isothermal sintering was carried out between 1100 and 1300 °C. Apparent density as high as 98% D_{th} was attained by firing isostatically pressed pellets at 1150 °C 4 h. Uniaxially pressed pellets attained the same apparent density at 1275 °C 2 h, being in both cases very low the densification temperatures. Microstructure was observed by scanning electron microscopy (SEM). Ionic conductivity was determined by complex impedance spectroscopy. Bulk and grain boundary conductivities have similar values, and the total conductivity attains good value compatible with the use as electrolyte in solid oxide fuel cell (SOFC).
© 2009 Elsevier Ltd. All rights reserved.

Keywords: Powders-chemical preparation; Sintering; Grain boundaries; Yttria-doped ceria; Ionic conductivity

1. Introduction

Rare earth doped ceria is a well-known electrolyte material for low temperature (500–700 °C) solid oxide fuel cell (SOFC) application due to their high oxygen ion conductivity at a lower temperature than that of the yttria-stabilised zirconia.[1–5] The main problem with these solid solutions is that they need to be sintered at very high temperatures, between 1500 and 1600 °C to attain moderate apparent densities, with the possibility of reduction of Ce(IV) to Ce(III).[6] A lot of work has been devoted to solve this problem: different routes to prepare reactive ceramic powder, such as coprecipitation, combustion synthesis, sol–gel formation, polymeric organic complex solution method, and others. With the same final objective, addition of some amounts of different oxides has been also essayed.[7–19]

Another problem associated to the final ceramic microstructure is the rather low conductivity of grain boundary, G.B. when compares with that of the corresponding bulk. This fact is attributed to the presence of impurities located in the G.B., which lowers the ionic mobility.[20] As consequence total conductivity suffers a considerable lowering. Several procedures have been suggested to overcome this fact: decreasing of the G.B. resistivity by increasing the grain size, i.e. lowering the G.B density, or incorporating controlled amount of some type of dopants that could clean the G.B. of non-adequate impurities.[21,22]

Ionic conductivity of rare-earth-doped ceria electrolytes depends of the rare-earth cation, being Sm and particularly Gd those which lead to a higher ionic conductivity.[23] Nevertheless, Y-doped ceria, which have a relatively high value of ionic conductivity is of particular interest due to the relative abundance and low cost of the yttrium element and its oxide against Sm and Gd. Because of this, a lot of work is being devoted to study solid electrolytes based on Y-doped CeO_2 (CeYCa in the following).[24–29] Dense electrolytes ($D_a \geq 95\%\ D_{th}$) have been reported.

The aim of the present paper is to obtain highly sinterable yttria-doped ceria, powders, with the following chemical composition: $Ce_{0.8}Y_{0.18}Ca_{0.02}O_{2-x}$, by a simple, cheap chemical procedure, such as coprecipitation of inorganic salts (nitrates), with a strict control of the variables, thus obtaining very homogeneous nanoscaled powder. Addition of 2 mol% CaO is driven to improve the G.B. conductivity by elimination–neutralization of impurities located in the G.B. particularly, SiO_2. Densification, microstructure and ionic conductivity will be measured.

* Corresponding author.
E-mail address: cmoure@icv.csic.es (C. Moure).

0955-2219/$ – see front matter © 2009 Elsevier Ltd. All rights reserved.
doi:10.1016/j.jeurceramsoc.2009.02.014

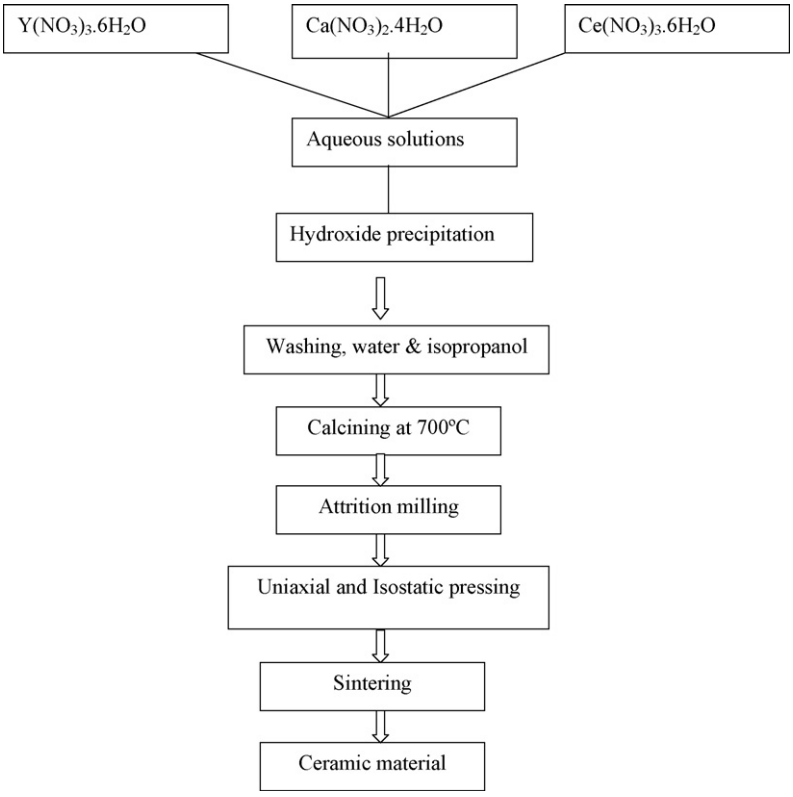

Fig. 1. Flow sheet of coprecipitation and synthesis process of CeYCa powders.

2. Experimental procedures

Ceria powders containing 18 mol% $YO_{1.5}$ and 2 mol% CaO were prepared by coprecipitation of hydroxides from an aqueous solution of the Ce, Gd and Ca nitrates ($Ce(NO_3)_3{\cdot}6H_2O$ (99.5%, Alfa Aesar), $Y(NO_3)_3{\cdot}6H_2O$ (99.9%, Alfa Aesar) and $Ca(NO_3)_2{\cdot}4H_2O$ (99.0%, Alfa Aesar)). The as-prepared aqueous transparent solution of the above nitrates was heated in air on a hot plate at about 80 °C with magnetic stirring in order to ensure the perfect dissolution and homogenization of the cationic precursors. Lately, this cerium–yttrium–calcium nitrate solution was added by dropping and blending to an ammonium hydroxide solution in excess, to maintain a pH 9 during the whole process, the mixed solution being vigorously stirred. When the precipitation process was apparently completed, an excess of NH_4OH was added for assure total precipitation; later the precipitate was slowly filtered. After filtering, the precipitate was first washed using distilled water, after several times

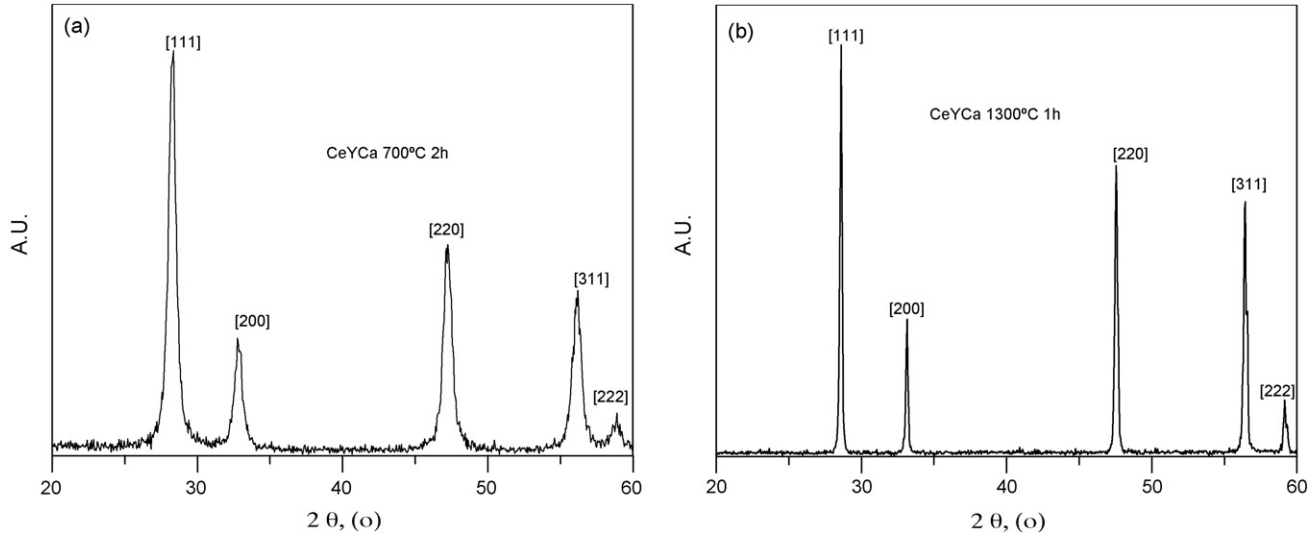

Fig. 2. XRD patterns of (a) calcined powders at 700 °C and (b) heat treated at 1300 °C.

with pure isopropanol (99.5%, Merck). The washed precipitate was slowly dried in a closed atmosphere at ≈60 °C, until total drying. Fig. 1 shows the flux sheet of the coprecipitation process. TG/ATD analysis was performed on the dried precipitate (no represented). According to the obtained results, the precursor was calcined at 700 °C, 2 h, temperature for which the weight losses have concluded. The calcined powder was attrition milled with isopropanol as liquid medium. The physicochemical characteristics of the calcined powders were determined by Coulter (Laser Coulter LS130 de Malvern Instruments (G.B.), BET (Quantachrome MS-16 model, Syosset, NY) and XRD diffraction (Siemens D-5000, Erlangen, Germany), and crystallite size was determined by line-broadening analysis of the XRD patterns.

Powder was uniaxially and isostatically pressed. Both procedures were made for establishing if there is a strong difference in the final sintering step between both compaction methods. Pore size distribution of as-pressed compacts was determined by mercury penetration porosimetry (Micromeritics, Autopore II, 9215, Norgross, USA). Constant heating rate (CHR) essays were performed on a Dilatometer (Netzsch 402E of Geratebau, Bayern, Germany), from room temperature up to 1500 °C at a constant heating rate of 5 °C/min. Isothermal sintering was conducted at several temperatures between 1100 and 1325 °C and times of 1–8 h. Apparent density was measured by water displacement. XRD analysis was carried out for determining the complete solid solution formation and crystallisation of the ceramic bodies. Lattice parameter of the solid solution was measured from all the peaks obtained with a scanner rate of 1/8 2θ/min between 20 and 60° 2θ, and using Si as internal standard. Microstructure was observed by SEM of polished and thermally etched surfaces. Ag paste was applied on the surface of sintered discs. Electrodes were fired at 750 °C 1 h; surface resistance values lower than 0.1 Ω were attained on the fired electrodes. Complex impedance spectroscopy was employed for determining bulk, G.B. and total ionic conductivity at a temperature range between 200 and 600 °C, and 10–10^7 Hz frequency range, by using a HP 4192A impedance meter. Conductivity values represented in the spectroscopic diagrams have been calculated from impedance data taken on the bulk and G.B. arcs by the formula $\sigma = (1/Z')(l/S)$, being l and S thickness and surface respectively measured on the disc samples. The value $\sigma = (1/Z'_{GB})(l/S)$ has been taken as average G.B. value for the shake of comparison between different samples and as representative of the electrical G.B behaviour of the ceramic electrolyte.

3. Results and discussion

Fig. 2a and b shows the XRD pattern of the calcined and 1300 °C-heat treated powders. The XRD patterns have been compared with the JCPDS file 75–175, corresponding to the same Y-doped ceria solid solution. Lattice parameter, measured on powder treated at 1300 °C, with a high degree of crystallinity gave a value $a = 0.54213 \pm 0.00005$ nm, and the theoretical density calculated for such a lattice parameter and the corresponding chemical formulae was $D_{th} = 6.63$ g/cm^3. The crystallite size (D) of the powder was calculated, using several diffraction lines,

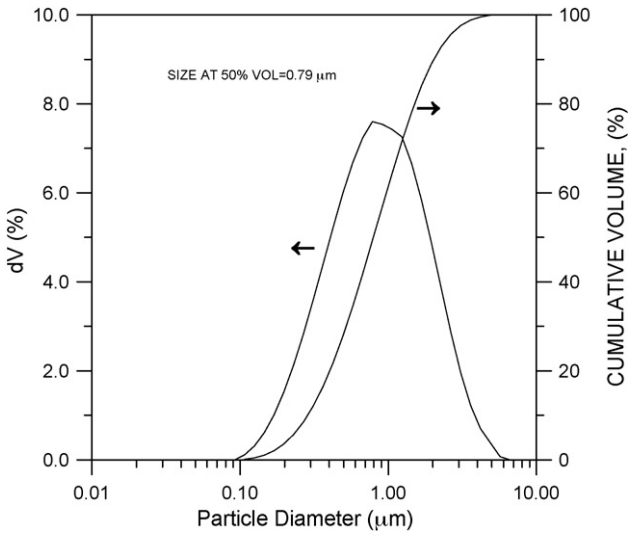

Fig. 3. Particle size curves taken by Laser Coulter, showing the agglomerates distribution of calcined CeYCa powders.

Table 1
Apparent density as a function of compaction pressure.

Sample	Apparent density (%)			
	Uniaxial (2000 MPa)	Isostatic (1500 MPa)	Isostatic (2000 MPa)	Isostatic (2500 MPa)
1150 °C 2 h	94 ± 0.5	97.3 ± 0.5	98.1 ± 0.5	98.1 ± 0.5
1275 °C 2 h	98 ± 0.5	95.5 ± 0.5	94.7 ± 0.5	93.5 ± 0.5

from the Scherrer formula, $D = 0.9\lambda/\beta \cos\theta$, where λ is the wavelength of X-rays, β the corrected half-width line, that is obtained using the (1 1 1) line of the pure silicon as the standard, and θ the angle corresponding to the analyzed line. Values of $D = 24$ nm were calculated. Specific surface area was 45 m^2/g, which is equivalent to 20 nm calculated from the formula $D_s = 6/SD_{th}$,

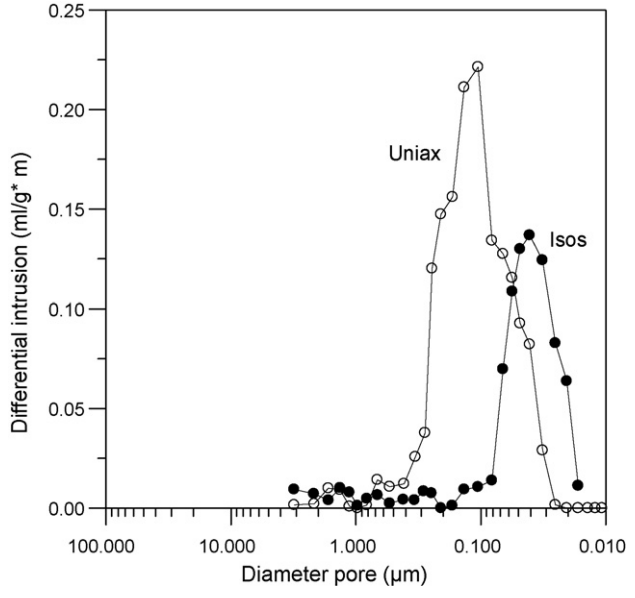

Fig. 4. Pore size distribution in green, uniaxially and isopressed, compacts.

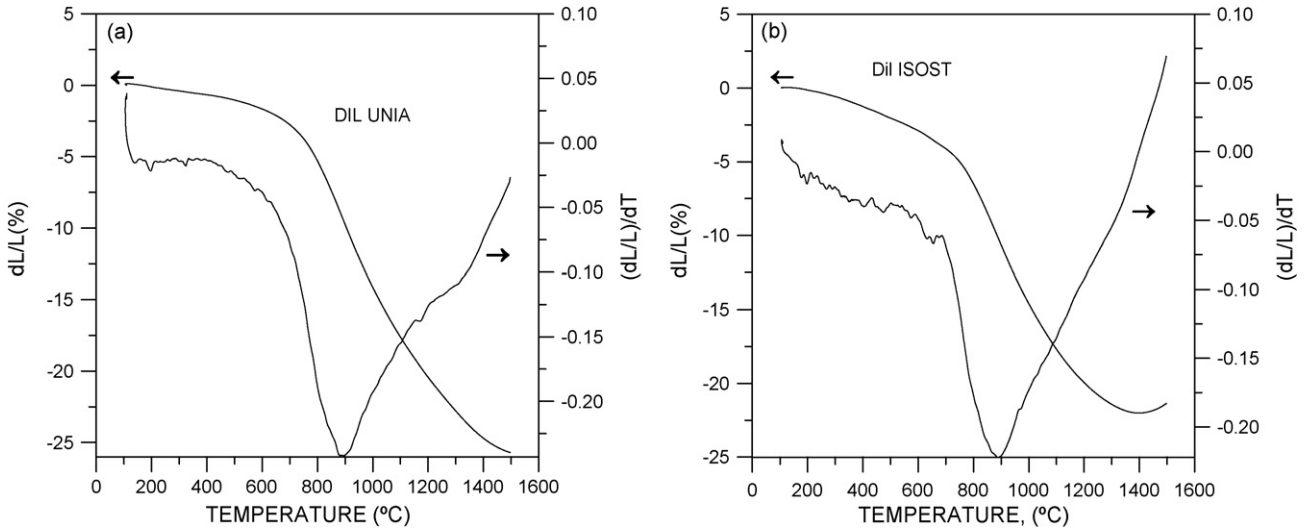

Fig. 5. Shrinkage and shrinkage rate curves corresponding to (a) uniaxially pressed compacts and (b) isopressed (2000 MPa) compacts.

in good concordance with the calculated by XRD line profile. Values obtained from particle size measurement by Coulter technique, see Fig. 3, gave mean particle size of 0.78 μm, which seem to correspond to a certain agglomeration degree and not a real particle size. Table 1 summarizes the physical parameters of the calcined powder.

Fig. 4 shows the pore-size distribution curves for the green compacts. As it is possible to see, pore distribution is very narrow and homogeneous for both type samples, uniaxially and isostatically pressed, being something wider for uniaxially pressed pellets.

Fig. 5a and b shows shrinkage and shrinkage rate curves for both uniaxially and isopressed samples. There is a difference between both samples: whereas the isostatically pressed sample ends its shrinkage step at 1380 °C and then suffers an apparent de-sintering process, with a slight expansion until 1500 °C, uniaxially pressed sample has not completed its shrinkage step at 1500 °C. On the other hand, shrinkage rate curves are very similar, with a single maximum at temperatures very near between them, 888.5 and 894.1 °C respectively, in good correlation with the near pore size and distribution curves shown for the two samples, Fig. 4. Thus, it is possible to attribute the different shrinkage behaviour to an existing difference between the green densities of the samples caused by the different compaction procedure. Uniaxially pressed samples have lower green density. The powder is looser and the beginning of the shrinkage is therefore at a higher temperature. In the isopressed powder, once attained a maximum in the apparent density, a grain growth step begins,

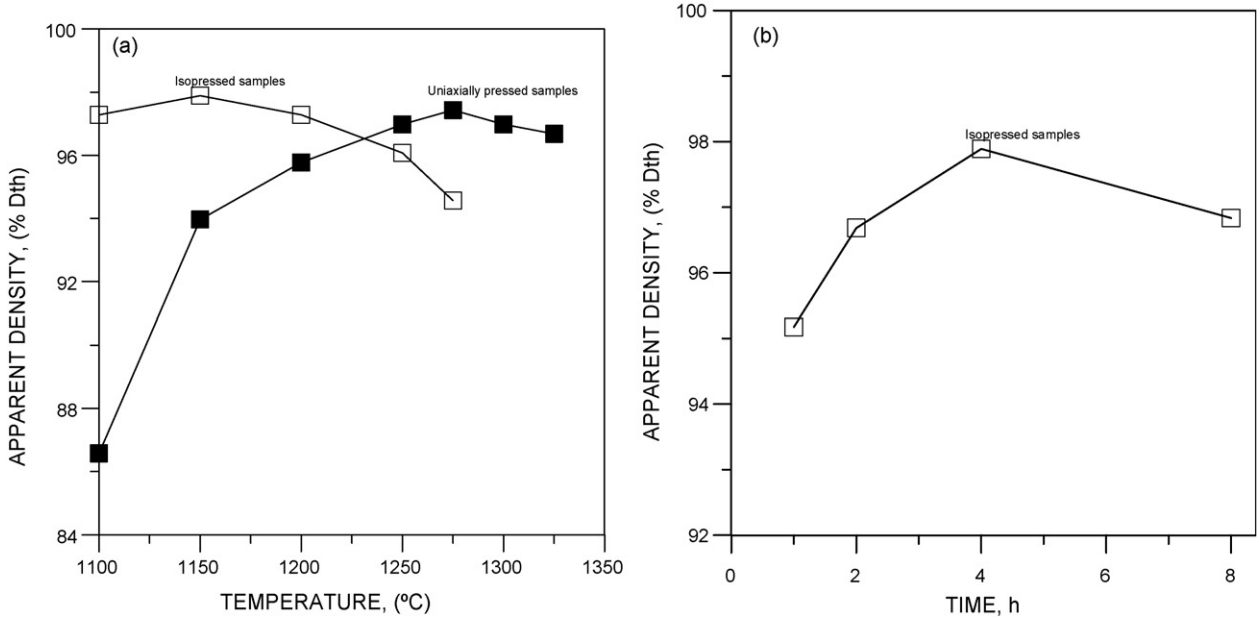

Fig. 6. Apparent density obtained by isothermal sintering at (a) different temperatures and constant time (2 h) (□ isopressed samples; ■ uniaxially pressed samples) and (b) different times at constant temperature, 1150 °C, for isopressed samples only.

Table 2
Apparent density as a function of compaction pressure.

Sample	Apparent density (%)			
	Uniaxial (2000 MPa)	Isostatic (1500 MPa)	Isostatic (2000 MPa)	Isostatic (2500 MPa)
1150 °C 2 h	94 ± 0.5	97.3 ± 0.5	98.1 ± 0.5	98.1 ± 0.5
1275 °C 2 h	98 ± 0.5	95.5 ± 0.5	94.7 ± 0.5	93.5 ± 0.5

which can be very fast, trapping the residual porosity and producing pore coalescence in the grain interior, with a bloating phenomena, which lowers the apparent density.[30] On the other hand, the slower reaction between the looser particles of the uniaxially pressed samples leads the final densification to a higher temperature.

According to the CHR results, isothermal sintering was carried out, taking as temperature range one beginning after the maximum rate of shrinkage, i.e. 1100 °C, and ending below 1400 °C. An essay about the influence of isostatically applied pressure has been made, in which 1500, 2000, and 2500 MPa have been applied. These samples have been sintered at 1150 °C 2 h, once known the optimal sintering temperatures. The results are compared with that obtained by uniaxially pressure.

Fig. 6a depicts the apparent density against temperature for 2 h soaking time for both isostatically at 2000 MPa and uniaxially pressed samples. There is a difference of 125 °C in the temperature of the maximum densification as a function of the pressing method. It is also important to notice that a density 98% D_{th} has been attained at 1150 °C, 4 h of soaking time, temperature well below of those found in the literature.[25,26] Fig. 6b shows the relative density of isopressed samples fired at 1150 °C, as a function of time, attaining the maximum of density at 4 h, followed by a de-sintering step, similar to that observed in the dilatometric essay above 1380 °C. Table 2 shows the apparent density of samples subjected to different compaction process. Such as can be observed, the pressure level has scarce influence above 2000 MPa, but the lowering of the pressure below this value causes that the final apparent density falls out.

Figs. 7–9 depict the microstructure of selected samples. Such as can be seen, microstructure corresponding to the sample sintered at 1150 °C, 2 h is near of a nanometric structure (Fig. 7a and b). Fig. 8 depicts microstructure of uniaxially pressed sample sintered at 1275 °C, which shows a submicronic grain size range. Even the sample sintered at 1500 °C (dilatometric essay) in which soaking time was null, shows a similar microstructural behaviour (Fig. 9) with small-grained microstructure.

Fig. 10 represents impedance arcs corresponding to well-densified 1150 °C 4 h isopressed sample. Such can be seen, bulk and G.B. arcs are of the same magnitude order, and in some extension both are overlapping, indicating that the G.B.

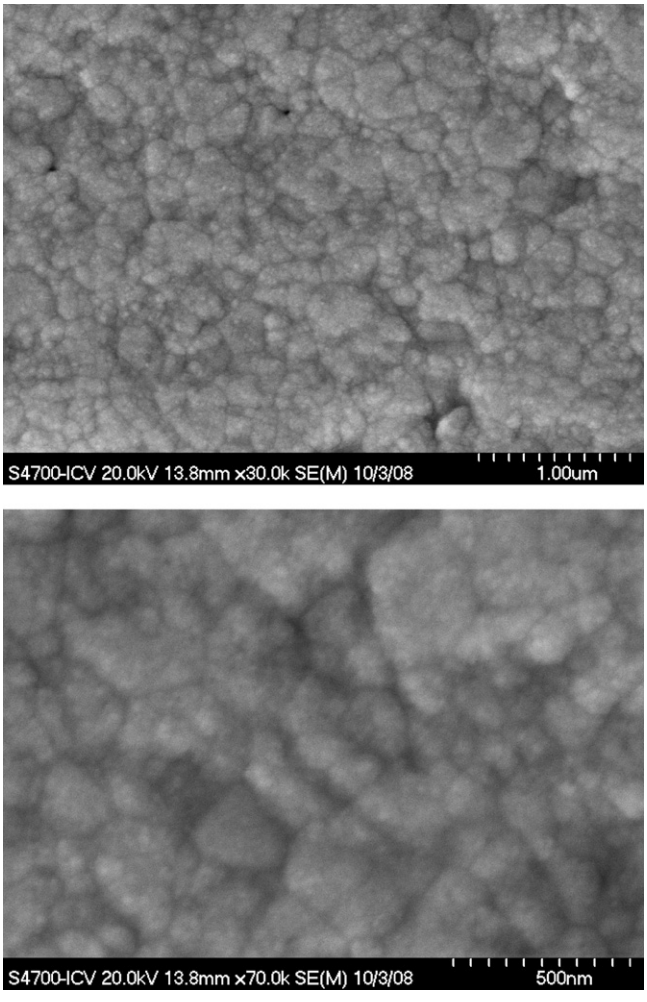

Fig. 7. SEM micrographs at different amplification of polished and thermally etched surfaces of sample fired at 1150 °C 4 h. Sample has been isopressed at 2000 MPa.

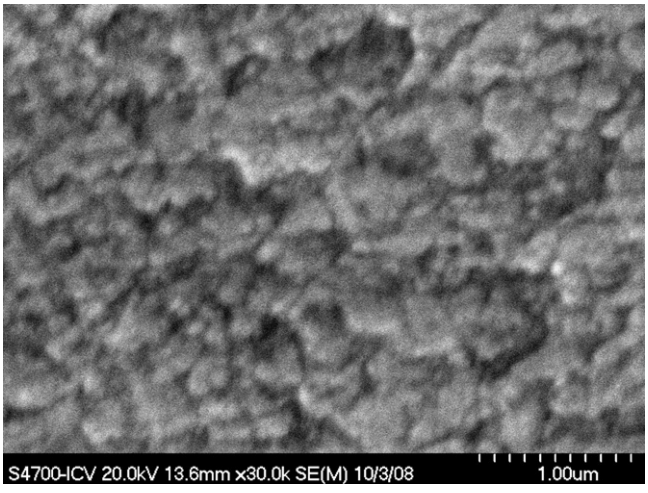

Fig. 8. SEM micrograph of polished and thermally etched surfaces of uniaxially pressed sample fired at 1275 °C 4 h.

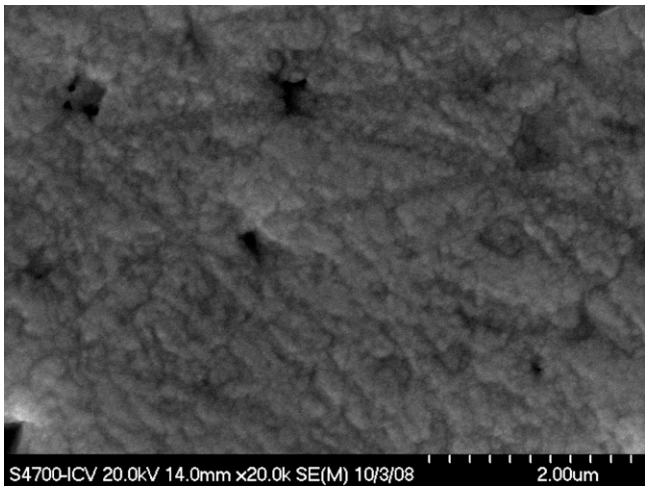

Fig. 9. SEM micrograph of polished and thermally etched surfaces of isopressed sample fired at 1500 °C. Dilatometric sample.

is comparable, although lower, to that of bulk one. As a mater of example, 277 °C arc is taken, in which the bulk resistivity has been measured as 436,410 Ω cm and the G.B resistivity is 523,800 Ω cm, which are of the same magnitude order

Fig. 11 shows the Arrhenius plots of bulk and G.B conductivity measured in both 1150 °C 4 h and 1500 °C dilatometric samples that present different density but with similar grain size, according to that seen in the microstructure.

It can be seen that the bulk and the G.B. conductivity values are not very different, and even in both cases the apparent G.B. conductivity is slightly higher than the bulk conductivity at temperatures enough high. As consequence, the total conductivity is not strongly different that the bulk conductivity, such as occurs in ceramics with high-resistivity Grain boundary behaviour. Lower values of conductivity, measured in the dilatometric sample can be attributed to lower apparent density of this sample.

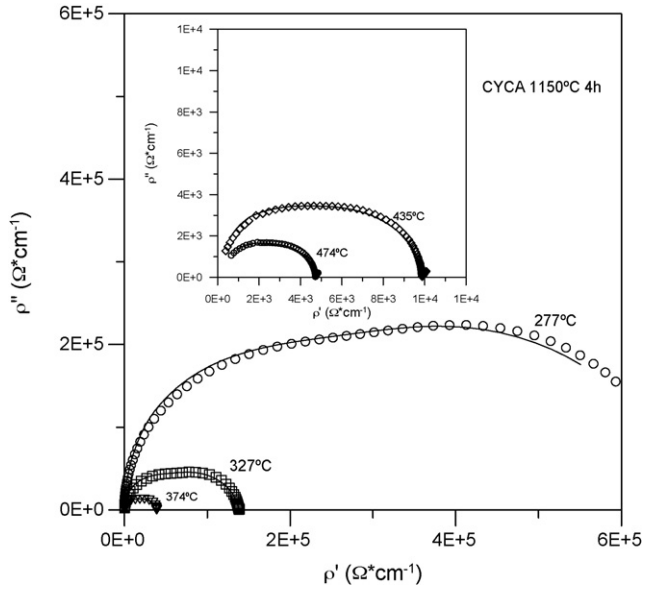

Fig. 10. Impedance arcs of sample fired at 1150 °C 4 h. Inset depicts the high-temperature region showing the corresponding arcs.

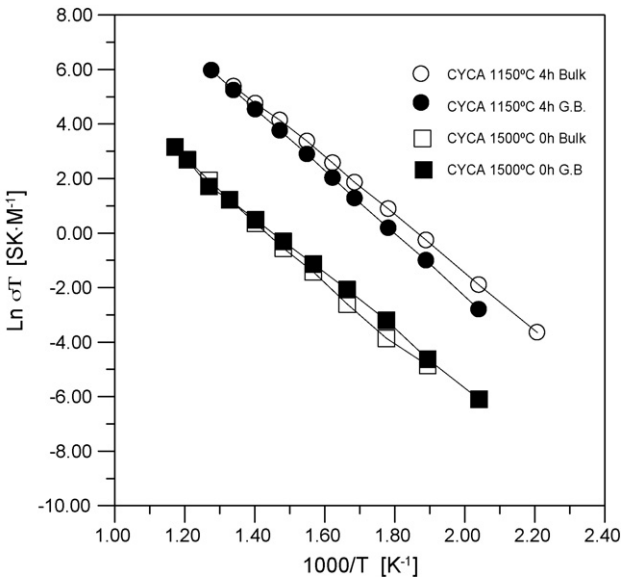

Fig. 11. Arrhenius plots of log ρ against $1/T$ of samples sintered at 1150 °C 4 h 1500 °C, dilatometric sample.

Taking into account that the bulk conductivity is very high, the falling in the G.B. conductivity caused by possible impurity phases is more notorious that in the YSZ electrolytes. As a solution to this problem it has been proposed the use of raw materials with very high purity.[29] Nevertheless, this solution is very little practical due to the strong increase of the raw materials costs. Besides that, control of the processing step is needed because of the possible incorporation of new impurities during that process. In some cases, high-resistivity G.B has been reported in very pure samples, indicating formation of a space charge layer.[31] Such as have been shown in the above exposed results, incorporation of controlled doping, which combines with G.B impurity and moving it towards triple points is a better and cheaper method to neutralize the impurity effects, These procedure was proved with success in Ceria-gadolinia electrolytes.[21,22]

The total conductivity value for CeYCa-20 sample fired at 1150 °C 4 h, with apparent density of 98 D_{th}, measured at 500 °C is 3.15×10^{-1} S M^{-1}.

4. Summary

Controlling the processing parameters of the chemical process: pH, coprecipitation rate, washing, drying, and temperature of synthesis leads to obtain sinterable CeYCa nanopowders, homogeneous and poorly agglomerated, which allows sintering at near theoretical density at temperatures as low as 1150 °C and times, of 2–4 h, attaining submicronic, near nanometric, structures, by using an improved hydroxide coprecipitation procedure. Addition of small amount of CaO, 2 mol% improves the grain boundary conductivity, and therefore, the total ionic conductivity of ceramic bodies. These materials are promising as solid electrolytes due to its low temperature sintering, which inhibited the redox reaction $Ce^{4+} \leftrightarrow Ce^{3+}$, and its good total ionic conductivity.

Acknowledgement

This work was supported by PROFIT project CIT-120000-2007-2010.

References

1. Esposito, V. and Traversa, E., Design of electroceramics for solid oxides fuel cell applications: playing with ceria. *J. Am. Ceram. Soc.*, 2008, **91**(4), 1037–1051.
2. Steele, B. C. H., Appraisal of $Ce_{1-y}Gd_yO_{2-y/2}$ electrolytes for IT-SOFC operation at 500 °C. *Solid State Ionics*, 2000, **129**, 95–110.
3. Gödickemeier, M. and Gauckler, L. J., Engineering of solid oxide fuel cells with ceria-based electrolytes. *J. Electrochem. Soc.*, 1998, **145**(2), 414–421.
4. Herle, J. V., Horita, T., Kawada, T., Sakai, N., Yokokawa, H. and Dokiya, M., Fabrication and sintering of yttria-doped ceria powder. *J. Am. Ceram. Soc.*, 1997, **80**, 933–940.
5. Yahiro, H., Eguchi, K. and Arai, H., High temperature fuel cell with ceria-yttria solid electrolyte. *J. Electrochem. Soc.*, 1988, **135**, 2077–2080.
6. Aneggi, E., Boaro, M., de Leitenburg, C., Dolcetti, G. and Trovarelli, A., Insights into the redox properties of ceria-based oxides and their implications in catalysis. *J. Alloy Compd.*, 2006, **408–412**, 1096–1102.
7. Duran, P., Moure, C. and Jurado, J. R., Sintering and microstructural development of ceria-gadolinia dispersed powders. *J. Mater. Sci.*, 1994, **29**, 1940–1948.
8. Chen, P. L. and Chen, I.-W., Reactive cerium (IV) oxide powders by the homogeneous precipitation method. *J. Am. Ceram. Soc.*, 1993, **76**(6), 1577–1583.
9. Highasi, K., Sonoda, K., Ono, H., Sameshima, S. and Hirata, Y., Synthesis and sintering of rare-earth-doped ceria powder by the oxalate coprecipitation method. *J. Mater. Res.*, 1999, **14**(3), 957–967.
10. Zhang, T. S., Ma, J., Kong, L. B., Hing, P. and Kilner, J. A., Preparation and mechanical properties of dense $Ce_{0.8}Gd_{0.2}O_{2-d}$ ceramics. *Solid State Ionics*, 2004, **167**, 191–196.
11. Go, Y. B. and Jacobson, A. J., Solid solution precursors to gadolinia-doped ceria prepared via a low-temperature solution route. *Chem. Mater.*, 2007, **19**, 4702–4709.
12. Durán, P., Capel, F., Gutierrez, D., Tartaj, J. and Moure, C., Cerium (IV) oxide synthesis and sinterable powders prepared by the polymeric organic complex solution method. *J. Eur. Ceram. Soc.*, 2002, **22**, 1711–1721.
13. Rocha, R. A. and Muccillo, E. N. S., Physical and chemical properties of nanosized powders of gadolinia-doped ceria prepared by the cation complexation technique. *Mater. Res. Bull.*, 2003, **38**, 1979–1986.
14. Choi, K.-H., Choi, Y.-G., Park, M.-W., Kodash, V. Y., Groza, J. R. and Lee, J.-S., Effects of alumina additions on sintering behavior of $Ce_{0.8}Sm_{0.2}O_{1.9}$ ceramics synthesized by Pechini method. *J. Alloys Compd.*, 2008, **463**, 484–487.
15. Maca, K., Cihlar, J., Castkova, K., Zmeskal, O. and Hadraba, H., Sintering of gadolinia-doped ceria prepared by mechanochemical synthesis. *J. Eur. Ceram. Soc.*, 2007, **27**, 4345–4348.
16. Zhang, Z., Sigle, W., Rühle, M., Jud, E. and Gauckler, L. J., Microstructure characterization of a cobalt-oxide-doped cerium-gadolinium-oxide by analytical and high-resolution TEM. *Acta Mater.*, 2007, **55**, 2907–2917.
17. Jud, E., Huwiler, C. B. and Gauckler, L. J., Sintering analysis of undoped and Cobalt oxide doped Ceria solid solutions. *J. Am. Ceram. Soc.*, 2005, **88**(11), 3013–3019.
18. Lee, J.-S., Choi, K.-H., Ryu, B.-K., Shin, B.-C. and Kim, I.-S., Effects of gallia additions on sintering behavior of gadolinia-doped ceria. *Mater. Res. Bull.*, 2004, **39**, 2025–2033.
19. Gil, V., Tartaj, J., Moure, C. and Duran, P., Rapid densification by using Bi_2O_3 as an aid for sintering of gadolinia-doped ceria ceramics. *Ceram. Int.*, 2007, **33**, 471–475.
20. Guo, X., Sigle, W. and Maier, J., Blocking grain boundaries in yttria-doped and undoped ceria ceramics of high purity. *J. Am. Ceram. Soc.*, 2003, **86**(1), 77–87.
21. Cho, Y. H., Cho, P.-S., Auchterlonie, G., Kim, D. K., Lee, J.-H., Kim, D.-Y., Park, H.-M. and Drennan, J., Enhancement of grain-boundary conduction in gadolinia-doped ceria by the scavenging of highly resistive siliceous phase. *Acta Mater.*, 2007, **55**, 4807–4815.
22. Cho, P.-S., Lee, S. B., Cho, Y. H., Kim, D.-Y., Park, H.-M. and Lee, J.-H., Effect of CaO concentration on enhancement of grain-boundary conduction in gadolinia-doped ceria. *J. Power Sources*, 2008, **183**, 518–523.
23. Pascual, C., Del Olmo, L., Jurado, J. R., Arroyo, G. F., Moure, C. and Duran, P., Electrical conductivity of solid solutions in the systems CeO_2–CaO and CeO_2–Ln_2O_3 (Ln = La, Nd, Sm, Gd, Er, Y. *Sci. Ceram.*, 1983, **12**, 729–734.
24. Yahiro, H., Baba, Y., Eguchi, K. and Arai, H., High temperature fuel cell with ceria–yttria solid electrolyte. *J. Electrochem. Soc.*, 1988, **135**, 2077–2080.
25. Ma, J., Zhang, T. S., Kong, L. B., Hing, P., Leng, Y. J. and Chan, S. H., Preparation and characterization of dense $Ce_{0.85}Y_{0.15}O_{2-\delta}$ ceramics. *J. Eur. Ceram. Soc.*, 2004, **24**, 2641–2648.
26. Xu, H., Yan, H. and Chen, Z., Sintering and electrical properties of $Ce_{0.8}Y_{0.2}O_{1.9}$ powders prepared by citric acid-nitrate low-temperature combustion process. *J. Power Sources*, 2006, **163**, 409–414.
27. Li, J.-G., Wang, Y., Ikegami, T. and Ishigaki, T., Densification below 1000 °C and grain growth behaviour of yttria doped ceria ceramics. *Solid State Ionics*, 2008, **179**, 951–954.
28. Xu, H. M., Yan, H. G. and Chen, Z. H., Low-temperature combustion synthesis and sintering of nanosized $Ce_{0.8}Y_{0.2}O_{1.9}$ powders. *Mater. Charact.*, 2008, **59**, 301–305.
29. Tadokoro, S. K. and Muccillo, E. N. S., Influence of the precursor purity and the precipitating agent on impedance spectroscopy of CeO_2:Y_2O_3 ceramics. *J. Alloys Compds.*, 2004, **374**, 190–193.
30. Duran, P., Tartaj, J. and Moure, C., Sintering behaviour and microstructural evolution of agglomerated spherical particles of high-purity barium titanate. *Ceram. Int.*, 2003, **29**, 419–425.
31. Guo, X. and Waser, R., Electrical properties of the grain boundaries of oxygen ion conductors: acceptor-doped zirconia and ceria. *Progr. Mater. Sci.*, 2006, **51**, 151–210.